RSC Advances

PAPER

View Article Online
View Journal | View Issue

Cite this: *RSC Adv.*, 2020, **10**, 16982

Ratiometric temperature measurement using negative thermal quenching of intrinsic $BiFeO_3$ semiconductor nanoparticles†

Željka Antić, *[a] K. Prashanthi, *[b] Sanja Kuzman,[a] Jovana Periša,[a] Zoran Ristić,[a] V. R. Palkar[c] and Miroslav D. Dramićanin[a]

Received 28th February 2020
Accepted 15th April 2020

DOI: 10.1039/d0ra01896a

rsc.li/rsc-advances

A strategy for optical nanothermometry using the negative thermal quenching behavior of intrinsic $BiFeO_3$ semiconductor nanoparticles has been reported here. X-ray diffraction measurement shows polycrystalline $BiFeO_3$ nanoparticles with a rhombohedral distorted perovskite structure. Transmission electron microscopy shows agglomerated crystalline nanoparticles around 20 nm in size. Photoluminescence measurements show that intensity of the defect level emission increases significantly with temperature, while the intensity of near band emission and other defect levels emissions show an opposite trend. The most important figures of merit for luminescence nanothermometry: the absolute (S_a) and the relative sensor sensitivity (S_r) and the temperature resolution (ΔT_m) were effectively resolved and calculated. The relative sensitivity and temperature resolution values are found to be 2.5% K^{-1} and 0.2 K, respectively which are among the highest reported values observed so far for semiconductors.

Introduction

For 80% of all sensors on the global market, temperature is the most frequently measured physical quantity. Many types of thermometers are currently being used including thermocouples, thermistors, liquid-in-glass, bimetallic, resistance, manometric and infrared thermometers.[1,2]

Scientific and technological progress creates an ongoing need for the development of new measuring concepts and instruments. There is now an immediate need for non-contact thermometry of moving or contact-sensitive objects, bodies that are difficult to access or in hazardous locations. Temperature measurements resulting from changes in materials' optical properties are considered as a promising route to meet the needs. Raman scattering, optical interferometry, thermoreflectance, near-field scanning optical microscopy and photoluminescence (PL) spectroscopy are the optical methods of interest.[1]

Temperature strongly affects photoluminescence features of optical materials such as peak energy and intensity, band shape, excited states lifetimes, and rise-times, which can be exploited to measure temperature. The temperature read-out method most commonly used in the present practice of luminescence thermometry is one based on the determination of the ratio of intensities of different emission bands of luminescent material. Ratiometric measurements are self-referencing and prone to fluctuations in excitation sources and detection electronics.[1]

To date, luminescence-based nanothermometry has been performed mainly using organic dyes, lanthanides (Ln) and transition metal (TM)-doped nanoparticles, and semiconductor quantum dots (QDs). In recent years researchers have started to explore the potential of luminescent materials' negative thermal quenching effect for non-contact temperature sensing. Lei *et al.* showed in a series of $NaGdF_4$@Ca/Yb/Er:$NaGdF_4$ core–shell nanocrystals that confining doping ions in two-dimensional space and introducing defect energy level *via* low-valence doping benefit the negative thermal quenching effect in the upconversion nanocrystals.[3] Zou *et al.* reported a strategy for enhancing photon upconversion at high temperatures by taking advantage of negative thermal expansion host materials. They reported a 29-fold enhancement of green upconversion luminescence in the Er^{3+}-doped orthorhombic $Yb_2W_3O_{12}$ crystals when temperature is increased from 303 to 573 K.[4] Also, authors have focused on uncommon thermal quenching effects in thermochromic materials and Covalent Organic Frameworks (COF). Mazza *et al.* have shown that the spontaneous opening and closing of oxazine heterocycles might become a viable mechanism to design fluorescence sensors capable of responding ratiometrically to temperature.[5] Kaczmarek *et al.* have proposed a new class of materials, Ln^{3+}-grafted Covalent Organic Frameworks (LnCOF), employed for temperature

[a]*University of Belgrade, Vinča Institute of Nuclear Sciences, P.O. Box 522, Belgrade, Serbia. E-mail: zeljkaa@gmail.com*

[b]*University of Alberta, Department of Chemical & Materials Engineering, Edmonton, Canada. E-mail: kovur@ualberta.ca*

[c]*Indian Institute of Technology Bombay (IIT-B), Mumbai, India*

† Electronic supplementary information (ESI) available. See DOI: 10.1039/d0ra01896a

sensing applications. In Eu/Tb systems they observed a quite unusual and rarely reported behavior in which there is no thermal quenching of the Tb^{3+} emission, as a result of the absence of ion-to-ligand/host energy back transfer.[6]

In semiconductors, the intensity of photoluminescence normally decreases with higher temperature (thermal quenching) mainly due to thermally-induced delocalization of charge carriers followed by non-fluorescent trapping.[7,8] Here, an approach for monitoring temperature variations using defect emission from intrinsic semiconductor $BiFeO_3$ (BFO) nanoparticles (NPs) is reported. Generally, materials made up of nanoparticles have a larger surface area when compared to the same volume of material made up of larger particles. It means that the surface-to-volume ratio increases as the radius of the sphere decreases. In BFO nanostructures, surface states play a vital role in optical and electrical characteristics due to the high surface-to-volume ratio when compared with bulk material.[9–12] They serve as traps for carriers and hence affect the recombination and transport of charge carriers.[13–16] Unlike conventional optical thermometry with semiconductors where luminescent signal decreases at high temperatures, we have observed that BFO NPs exhibit an emission-related negative thermal quenching (NTQ), where the photoluminescence intensity increases with temperature. Here, we propose strategy for temperature sensing based on the NTQ mechanism of intrinsic BFO NPs with an excellent performance of thermal sensitivity and resolution.

Experimental part

Materials

Bismuth(III) nitrate pentahydrate (98%) and 2-methoxyethanol (99+%) were purchased from Acros Organics and used as received. Ferric nitrate nonahydrate (99.99%) was purchased from Sigma Aldrich and used as received.

Preparation of semiconductor BFO NPs

Semiconductor BFO NPs were prepared *via* sol–gel route. BFO solution (sol) has been prepared by mixing bismuth(III) nitrate pentahydrate and ferric(III) nitrate nonahydrate in a molar ratio of 1.05 : 1 in 2-methoxyethanol as a solvent. The precursor solution was stirred at 80 °C for one hour, after which a reddish sol was recovered. The solution was dried at 100 °C for 2 h in vacuum to obtain BFO xerogel powder which was then ground in a crucible, and annealed at 600 °C for 2 h in the air.

Characterization

The size of the BFO NPs was analysed using transmission electron microscopy (TEM) (JEOL JEM-2100).

Structural analysis of BFO NPs was done by X-ray diffraction measurements on a Rigaku X-ray diffractometer using Cu Kα radiation ($\lambda = 1.546$ Å).

The PL thermometry data were collected using a Fluorolog-3 Model FL3-221 spectrofluorometer system (Horiba-Jobin-Yvon) over the temperature range from room temperature (RT = 293 K) to 453 K under continuous excitation using 450 W xenon lamp ($\lambda_{ex} = 320$ nm). Time-resolved PL measurements were acquired utilizing a Xenon–Mercury pulsed lamp as excitation source. For PL measurements, the BFO NPs were prepared in a form of pallet. The BFO NPs pallet was placed on a custom-made temperature controlled furnace, and emission spectra were collected *via* an optical fiber bundle. The temperature of the samples was controlled within the accuracy of ±0.5 K by a temperature control system utilizing a proportional-integral-derivative feedback loop equipped with the T-type thermocouple for temperature monitoring.

Results and discussion

Morphological and structural characterization of BFO NPs

Transmission electron microscopy shows agglomerated crystalline nanoparticles with variable dimensions in 10–50 nm range and boundary lines observed clearly in some regions (Fig. 1(a)). Fig. 1(b) depicts a TEM image of a single BFO NPs around 20 nm in size. The interplanar spacing observed from Fig. 1(c) is about 0.374 nm for (012) and 0.278 nm for (104) planes. The obtained lattice spacing is in a close agreement with the literature values for BFO nanostructures.[17,18]

The XRD pattern, Fig. 1(d), corresponds to polycrystalline BFO of the R3C rhombohedral distorted perovskite structure (ICDD 01-070-5668), and no noticeable diffractions can be observed for impurity phases. The average crystallite size of ~30 nm was estimated from the full widths at half maximum (FWHMs) of the resolved reflections in the X-ray powder diffraction pattern using the Debay-Scherrer approximation. A Scherrer constant of $K = 0.89$ was taken as an average for every reflection although it was shown that this constant is anisotropic and its value may vary for different (*hkl*).[19]

One should note that the X-ray diffraction is a structural technique that provides the analysis at a micron scale, while the TEM reveals the structure and morphology at the atomic level (Fig. 1(c)). Therefore, the calculated average crystallite size of ~30 nm from the XRD is in agreement with the 10 to 50 nm particle size obtained from TEM measurements.

By preparing the material with no traces of impurity phases, one can be ascertain in the reproducibility of photoluminescent measurements and, therefore, in the usability of the material as a luminescent thermal probe.

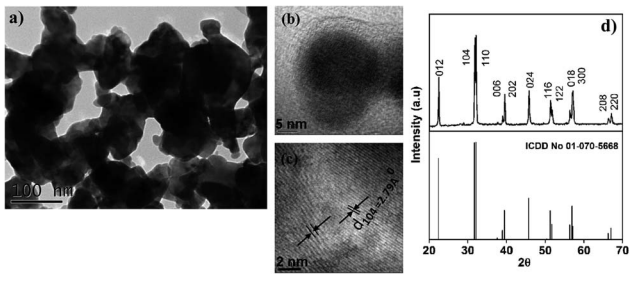

Fig. 1 (a) Low-magnification TEM image of a region with agglomerated BFO NPs; (b) HRTEM image of single nanoparticle; (c) high resolution TEM showing lattices spacing of BFO NPs and (d) XRD pattern of BFO NPs presented with corresponding ICDD card No. 01-070-5668.

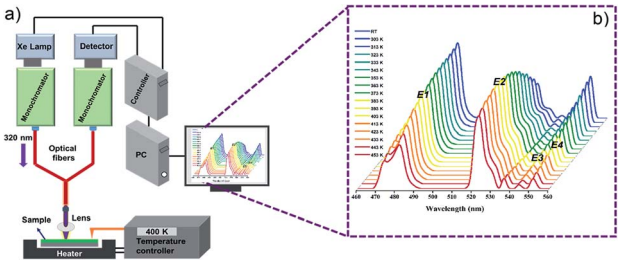

Fig. 2 (a) Experimental setup used for optical nanothermometry and (b) enlarged PL spectra of BFO nanoparticles over 293–453 K temperature range (temperature increment 10 K).

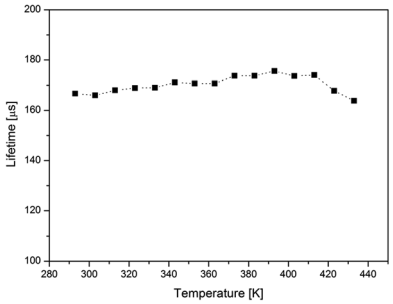

Fig. 4 Calculated lifetime values of the E2 emission as a function of temperature.

Temperature dependant BFO emission

Fig. 2 shows schematic illustration of used experimental setup and BFO NPs photoluminescence spectra obtained with increasing temperature from room to 453 K. Emission band with maxima at 482 nm (E1) corresponds to band edge/near band emission (NBE), while maxima at 523 nm (E2), 544 nm (E3) and 551 nm (E4) correspond to the defect level/surface state emissions (DLE). The emissions at 523 nm, 544 nm, and 551 nm are associated with oxygen vacancies (V_O) presence (more details are available in ESI, XPS, Fig. S1†).[10,11,20] The intensity of the defect level emission E2 (523 nm) increases significantly with temperature, while the intensity of near band emission E1 (482 nm) and other defect levels (E3, E4) emissions show an opposite trend (Fig. 3(A)). The intensity of the defect level emission E2 (523 nm) increases significantly with temperature, while the intensity of near band emission E1 (482 nm) and other defect levels (E3, E4) emissions show an opposite trend (Fig. 3(A)). The difference in the temperature dependence of band edge/near band (E1) and defect level/surface state (E2, E3, E4) emissions causes the change of probe's emission color from pale blue to light green, as shown in CIE color diagram in Fig. 3(B).

Oxygen vacancy related defect emissions and NTQ behavior has been reported in some oxide systems.[20–27] Moreover, in our previously published work on multifferoic BFO nanowires (NWs) reasonable interpretation of the photoluminescence NTQ process in BFO NWs and detailed representation of the energy levels and E1, E2, E3, and E4 bands is given.[15] Briefly, according to the multi-level model developed by Shibata[28] temperature dependent PL intensity can be expressed by activation energy for the process that increases the PL intensity with increasing temperature – NTQ (E_q') and activation energy for the non-radiative channels (E_j''). The activation energies of NTQ process (E_q') in BFO nanowires were found to be a few times greater for E2 than for E1, E3, and E4. Therefore, as temperature increases, the carriers with lower activation energy will start to escape into the barrier where they can recombine non-radiatively leading to decrease in the PL intensity while carriers with higher activation energy lead to NTQ behavior. In addition to recombination, one should note that energy states are closely spaced in energy so, according to Boltzmann distribution, redistribution of electron population between states exists and is higher at higher temperature (being proportional to kT). The E2 emission comes from the trap state of highest energy which is thermally coupled to lower E3 and E4 energy state. The increase in temperature is followed by a redistribution of electrons between the traps so that high-energy trap (E2) increases in population on account of lower-energy traps (E3 and E4).

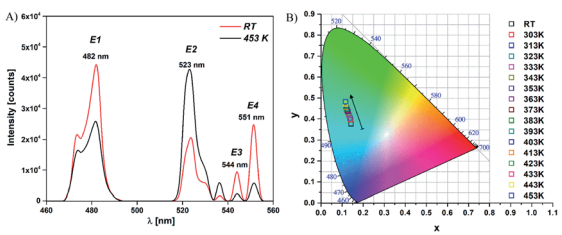

Fig. 3 (A) PL emission spectra of BFO NPs at RT (293 K) and at 453 K (λ_{ex} = 320 nm) and (B) CIE diagram of the BFO NPs in the RT – 453 K temperature range.

Temperature dependent luminescence decay lifetime

Due to the fact that the transitions from surface states are forbidden, the emission rate is slow and characterized by relatively high decay time (~170 μs). Fig. 4 presents calculated lifetime values of the E2 emission as a function of temperature. Similar to BFO NWs, the lifetime is independent of the temperature change, resembling the static quenching behavior and can be explained in terms of multiple trapping and de-trapping process.[15]

Temperature sensing based on ratiometric method

Since BFO NPs provide multiple emission peaks, a ratiometric approach to luminescence thermometry could be used. Such ratiometric measurements are insensitive to fluctuations of excitation source light or other changes in measurement conditions and, therefore, act as self-referencing (*i.e.*, measurements do not have to be referenced with any temperature standard).[1] Fig. 5(A) shows maximum PL intensity as a function of temperature for all four transitions while Fig. 5(B) shows a plot of the temperature dependence of the fluorescence intensity ratio (FIR) obtained as a ratio of E2 emission with other three (E1, E3, and E4).

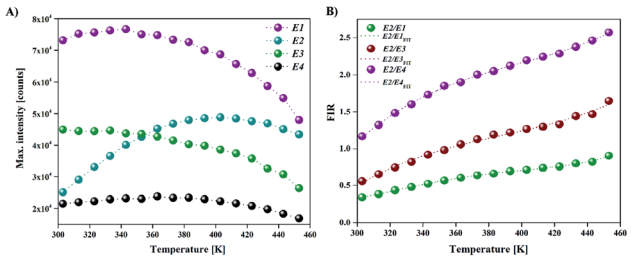

Fig. 5 (A) Maximum PL intensities as a function of temperature for all four transitions (E1, E2, E3, E4) and (B) fluorescence intensity ratio (FIR) values of BFO NPs as a function of temperature. FIR values were obtained as the ratio between peak intensities for E1, E3 and E4 with respect to E2.

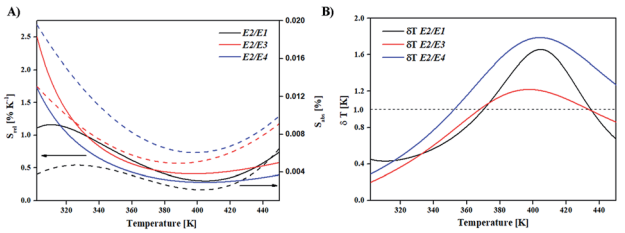

Fig. 6 (A) Relative (solid line) and absolute (dashed line) sensitivity of FIR thermometry and (B) temperature resolution.

The most important figures of merits for luminescence nanothermometry are: the absolute sensor sensitivity, S_a, defined as the slope of the signal change with temperature; the relative sensor sensitivity, S_r, defined as the normalized absolute sensor sensitivity with respect to the measured value and the temperature resolution (ΔT_m) indicating the minimum temperature that can be effectively resolved (where σ represents the uncertainty of the FIR measurement, here 0.5):[29]

$$S_a = \left|\frac{\partial \mathrm{FIR}}{\partial T}\right| = \mathrm{FIR} \times \frac{\Delta E}{kT^2}\left[\mathrm{K}^{-1}\right] \quad (1)$$

$$S_r = 100\% \times \left|\frac{1}{\mathrm{FIR}}\frac{\partial \mathrm{FIR}}{\partial T}\right| = 100\% \times \frac{\Delta E}{kT^2}\left[\%\ \mathrm{K}^{-1}\right] \quad (2)$$

$$\Delta T_{\min} = \frac{\sigma}{S_a}[\mathrm{K}] \quad (3)$$

The absolute and relative sensitivities of BFO NPs, as well as temperature resolution calculated from eqn (1)–(3) are plotted in Fig. 6 and summarized in Table 1. The maximal value of the relative sensitivity of 2.5% K^{-1} is found at room temperature for E2/E3 ratio and the value decreases with temperature to 0.4% K^{-1} at 398 K. Relative sensitivities achieved with BFO NPs are among the highest recorded for semiconductor nanothermometers, but with larger measurement range (for a comparison see Table 2).

Estimated temperature resolutions (see Fig. 6(B)) were better than 1 K for all ratios and temperatures up to 350 K with 0.2 K maximal resolution at room temperature for E2/E3 ratio. Note that temperature resolution estimates were based on the standard deviation of measurements obtained from the equipment described in the experimental section. In practice, the resolution will depend on the used instruments and the measurement conditions.

Table 1 Table summarizing figures of merit of the luminescent thermometry using NTQ effect of E2 emission of BFO nanoparticles. T_m is the temperature at which S_r is maximum

		Thermal sensitivity	Temperature resolution	
FIR ratio	Temperature range; T_m (K)	S_a (K^{-1})	S_r (% K^{-1})	@ 293 K (K)
E2/E1	293–453 (293)	7.4×10^{-3}	1.1	0.45
E2/E3	293–453 (293)	1.3×10^{-2}	2.5	0.2
E2/E4	293–453 (293)	2×10^{-2}	1.7	0.3

Table 2 Figures of merit of luminescent molecular thermometers displaying, the temperature range (ΔT, K) with the temperature at which S_r is maximum (T_m, K); the maximum relative sensitivity values (S_r, % K^{-1}), and temperature resolution (K) obtained *via* ratiometric method

Semiconductor material/ form	T range (ΔT, K) with the T at which S_r is maximum (T_m, K)	Relative sensitivity (S_r, % K^{-1})	Resolution (K)	Reference
CdSe/NCs	82–280	0.44		8
ZnS-caped CdSe/anodized-aluminum paint QDs	100–500 (245)	1.3		30
CdSe–ZnS/QDs	287–316	1.6	0.3	31
CdSe–ZnS/QDs	278–313	1.3		32
ZnS–AgInS/NPs	293–353	1		33
CdSe/ZnS and CdTe/ZnS/ QDs	287–320 (320)	0.9		34
CdTe@NaCl/QDs	80–360 (199)	0.61		35
$BiFeO_3$/NPs	**293–453 (293)**	**2.5**	**0.2**	**Present work**

Conclusion

In conclusion, we have investigated negative thermal quenching of intrinsic BFO NPs. Multiple peaks in the emission spectrum of BFO NPs enables the use of ratiometric luminescence thermometry in the 293–453 K temperature range with the relative sensitivity 2.5% K^{-1} and temperature resolution of 0.2 K at room temperature which are higher than previously reported values observed for other semiconductor nanothermometers. Unlike conventional optical thermometry with semiconductors, negative thermal quenching of BFO NPs offers a new opportunity for developing temperature sensors with superior performance at higher temperatures.

Conflicts of interest

There are no conflicts to declare.

Acknowledgements

The authors from Vinča Institute of Nuclear Sciences acknowledge funding from the European Union's Horizon 2020 FET Open Program under grant agreement No. 801305, and from the Ministry of Education, Science and Technological Development of the Republic of Serbia.

Notes and references

1 M. Dramićanin, *Luminescence thermometry: methods, materials, and applications*, Woodhead Publishing, Cambridge, 1st edn, 2018.
2 P. R. N. Childs, *Practical temperature measurement*, Oxford: Butterworth–Heinemann, Oxford, 2001, p. 372.
3 L. Lei, J. Xia, Y. Cheng, Y. Wang, G. Bai, H. Xia and S. Xu, *J. Mater. Chem. C*, 2018, **6**, 11587–11592.
4 H. Zou, X. Yang, B. Chen, Y. Du, B. Ren, X. Sun, X. Qiao, Q. Zhang and F. Wang, *Angew. Chem., Int. Ed.*, 2019, **58**, 1–6.
5 M. M. A. Mazza, F. Cardano, J. Cusido, J. D. Baker, S. Giordani and F. M. Raymo, *Chem. Commun.*, 2019, **55**, 1112–1115.
6 A. M. Kaczmarek, Y. Y. Liu, M. K. Kaczmarek, H. Liu, F. Artizzu, L. D. Carlos and P. Van Der Voort, *Angew. Chem., Int. Ed.*, 2020, **59**, 1932–1940.
7 D. J. Garcia and J. G. Sole, Quantum dot fluorescence thermometry, in *Thermometry at the nanoscale: techniques and selected applications*, ed. L. D. Carlos and F. Palacio, RSC Nanosci. Nanotechnol., 2016, pp. 83–123.
8 L. Jethi, M. M. Krause and P. Kambhampati, *J. Phys. Chem. Lett.*, 2015, **6**, 718–721.
9 K. Prashanthi, A. Phani and T. Thundat, Resonator, *Nano Lett.*, 2015, **15**, 5658–5663.
10 K. Prashanthi, G. Thakur and T. Thundat, *Surf. Sci.*, 2012, **606**, L83–L86.
11 K. Prashanthi, R. Gaikwad and T. Thundat, *Nanotech*, 2013, **24**, 505710–505715.
12 K. Prashanthi, P. Dhandharia, N. Miriyala, R. Gaikwad, D. Barlage and T. Thundat, *Nano Energy*, 2015, **13**, 240–248.
13 J. Lagowski, C. L. Balestra and H. C. Gatos, *Surf. Sci.*, 1972, **29**, 213–229.
14 H. C. Gatos and J. Lagowski, *J. Vac. Sci. Technol.*, 1973, **10**, 130–135.
15 K. Prashanthi, Ž. Antić, G. Thakur, M. D. Dramićanin and T. Thundat, *Phys. Status Solidi RRL*, 2017, 1700352–1700356.
16 J. M. Moison and M. Bensoussan, *Rev. Phys. Appl.*, 1987, **22**, 293–297.
17 T. J. Park, G. C. Papaefthymiou, A. J. Viescas, A. R. Moodenbaugh and S. S. Wong, *Nano Lett.*, 2007, **7**, 766–772.
18 F. Huang, Z. Wang, X. Lu, J. Zhang, K. Min, W. Lin, R. Ti, T. T. Xu, J. He, C. Yue and J. Zhu, *Sci. Rep.*, 2013, **3**, 2907.
19 J. I. Langford and A. J. C. Wilson, *J. Appl. Crystallogr.*, 1978, **11**, 102–113.
20 H. He, Y. Wang, J. Wang and Z. Ye, *Phys. Chem. Chem. Phys.*, 2011, **13**, 14902–14905.
21 H. He, Z. Ye, S. Lin, B. Zhao, J. Huang and H. Tang, *J. Phys. Chem. C*, 2008, **112**, 14262–14265.
22 M. Watanabe, M. Sakai, H. Shibata, C. Satou, S. Satou, T. Shibayama, H. Tampo, A. Yamada, K. Matsubara, K. Sakurai, S. Ishizuka, S. Niki, K. Maeda and I. Niikura, *Phys. B*, 2006, **376–377**, 711–714.
23 Y. L. Zhao, Y. Sun, L. Q. Pan, K. S. Li and D. B. Yu, *Appl. Phys. Lett.*, 2013, **102**, 042404–042407.
24 W. K. Choi, C. Park, B. Angadi, Y. S. Jung and J. W. Choi, *J. Electroceram.*, 2009, **23**, 331–334.
25 A. B. Djurišić and Y. H. Leung, *Small*, 2006, **2**, 944–961.
26 S. F. Wuister, A. van Houselt, D. C. de Mello, D. Vanmaekelbergh and A. Meijerink, *Angew. Chem.*, 2004, **43**, 3029–3033.
27 S. F. Wuister, D. C. de Mello and A. Meijerink, *J. Am. Chem. Soc.*, 2004, **126**, 10397–10402.
28 H. Shibata, *Jpn. J. Appl. Phys., Part 1*, 1998, **37**, 550.
29 M. Quintanilla, A. Benayas, R. Naccache and F. Vetrone, Luminescent nanothermometry with lanthanide-doped nanoparticles, in *Thermometry at the nanoscale: techniques and selected applications*, ed. L. Carlos and F. Palacio, RSC Nanosci. Nanotechnol., 2016, pp. 124–166.
30 H. Sakaue, A. Aikawa and Y. Iijama, *Sens. Actuators, B*, 2010, **150**, 569–573.
31 P. A. S. Jorge, M. Mayeh, R. Benrashid, P. Caldas, J. L. Santos and F. Farahi, *Meas. Sci. Technol.*, 2006, **17**, 1032–1038.
32 G. W. Walker, V. C. Sundar, C. M. Rudzinski, A. W. Wun, M. G. Bawendi and D. G. Nocera, *Appl. Phys. Lett.*, 2003, **83**, 3555–3557.
33 Y. Matsuda, T. Torimoto, T. Kameya, T. Kameyama, S. Kuwabata, H. Yamaguchi and T. Niimi, *Sens. Actuators, B*, 2013, **176**, 505–508.
34 C. D. S. Brites, P. P. Lima, N. J. O. Silva, A. Millan, V. S. Amaral, F. Palacio and L. D. Carlos, *Nanoscale*, 2012, **4**, 4799–4829.
35 S. Kalytchuk, O. Zhovtiuk, S. V. Kershaw, R. Zboril and A. L. Rogach, *Small*, 2016, **12**, 466–476.

